JOURNAL OF GEOPHYSICAL RESEARCH: SPACE PHYSICS, VOL. 118, 7348–7359, doi:10.1002/2013JA019099, 2013

Two-component model of topside ionosphere electron density profiles retrieved from Global Navigation Satellite Systems radio occultations

Guillermo González-Casado,[1] J. Miguel Juan,[2]
Manuel Hernández-Pajares,[3] and Jaume Sanz[3]

Received 7 June 2013; revised 22 October 2013; accepted 22 October 2013; published 12 November 2013.

[1] A simple model for the topside ionosphere region is introduced and applied to fit radio-occultation-retrieved electron density profiles for altitudes above the F2 peak. The model considers two isothermal components representing the population of the O^+ (ionosphere component) and the H^+ (protonosphere component) ions. The purpose of the model is to achieve an accurate fit of the observed profiles in the topside ionosphere region while, at the same time, allowing a direct and simple derivation of two important ionospheric parameters, namely the O^+ vertical scale height and the upper transition height. Covering a time period of 1 year, the fits with the two-component model function are compared with those achieved with one-component functions commonly used in the literature and it is shown that the former provides significantly better fits than the later, with more than a factor of two improvement. The model predictions concerning: the correlation between the O^+ vertical scale height and the upper transition height, the altitude dependence of the vertical scale height of the electron density, and the quantitative contribution of the protonosphere to the total electron content are examined and shown to be consistent with the observations and with previous studies. It is concluded that the model provides a realistic description of the vertical distribution of the two main ion constituents of the topside ionosphere.

Citation: González-Casado, G., J. M. Juan, M. Hernández-Pajares, and J. Sanz (2013), Two-component model of topside ionosphere electron density profiles retrieved from Global Navigation Satellite Systems radio occultations, *J. Geophys. Res. Space Physics*, *118*, 7348–7359, doi:10.1002/2013JA019099.

1. Introduction

[2] Currently, there are different observational techniques for determining the vertical electron density profile of the Earth's ionosphere: topside satellite sounding, ground ionosondes, incoherent scatter radar, and radio occultation (RO) of GPS receivers on board low Earth orbit (LEO) satellites. Thanks to the launch of the COSMIC/FORMOSAT-3 (CF3) constellation of LEO satellites, ROs are able to provide almost global coverage of the Earth's ionosphere for altitudes well above the F2 layer peak.

[3] Several analytical functions have been used in the past to represent the altitude dependence of the electron density profile, $N_e(h)$, in the ionospheric layers, such as the Chapman and the Epstein profiles, and even a simple exponential function [e.g., *Stankov et al.*, 2011]. The negative inverse of the height derivative of $\ln N_e(h)$, usually referred to as the vertical scale height (VSH), is a parameter commonly employed not only to characterize the gradient of the electron density profile but also to link its shape with the dynamics, temperature, and composition of the ionosphere as a function of time, space, and geomagnetic conditions throughout detailed climatological analysis [*Lei et al.*, 2005; *Stankov and Jakowski*, 2006; *Liu et al.*, 2007a, 2008].

[4] On the other hand, it is well known that the composition of the ionosphere changes from O^+ dominated to H^+ dominated as the altitude increases. In this study, the O^+ population that dominates the ionosphere composition in the lower altitude regions above the F2 layer peak will be referred to as the ionosphere component and the H^+ population as the protonosphere component. Due to the difference between the ion masses of each component, the scale height for the protonosphere component is larger than that for the ionosphere component, and hence, with increasing altitude, the influence of the protonosphere component increases while the influence of the ionosphere component decreases. The altitude at which the two components have equal density is usually called the ionosphere upper transition height

[1]Departament de Matemàtica Aplicada 2, Universitat Politècnica de Catalunya, Barcelona, Spain.
[2]Departament de Física Aplicada, Universitat Politècnica de Catalunya, Barcelona, Spain.
[3]Departament de Matemàtica Aplicada 4, Universitat Politècnica de Catalunya, Barcelona, Spain.

Corresponding author: G. González-Casado, Departament de Matemàtica Aplicada 2, Universitat Politècnica de Catalunya, Edifici Omega, Campus Nord, Jordi Girona, 1–3, E-08034 Barcelona, Spain. (guillermo.gonzalez@upc.edu)

©2013. American Geophysical Union. All Rights Reserved.
2169-9380/13/10.1002/2013JA019099

(UTH). The protonosphere may have a strong influence over the topside ionosphere (TI) depending on local time, season, geomagnetic latitude, and solar activity [*Cueto et al.*, 2007; *Reinisch et al.*, 2007; *Yizengaw et al.*, 2008; *Yue et al.*, 2010]. Thus, the UTH is a parameter of great interest for ionospheric studies and also for the characterization of the physical coupling between the plasmasphere and the TI [*Webb et al.*, 2006; *Bilitza and Reinisch*, 2007; *Hysell et al.*, 2009].

[5] It is not straightforward to determine the O^+ scale height and the UTH from the observed $N_e(h)$. The usual procedure is as follows: a linear fit to the observed $\ln(N_e)$ in a limited altitude range above the F2 peak provides an estimate of the local VSH, which is considered to be the same as the scale height of the ionosphere (O^+) component. Subsequently, assuming that the O^+ density continues to decrease exponentially with altitude with a constant VSH, the value of the UTH can be derived from the observed $N_e(h)$ and the estimated values of the O^+ density [*Marinov et al.*, 2004; *Kutiev et al.*, 2006; *Kutiev and Marinov*, 2007; *Stankov et al.*, 2007; *Liu et al.*, 2008; *Sibanda and McKinnell*, 2011].

[6] However, this approach has several limitations. First, a given range of altitudes must be selected a priori to perform the fit leading to the derivation of the O^+ scale height. Typically, that range is fixed by choosing some allowed range for the gradient of $N_e(h)$ starting at the minimum gradient [see, e.g., *Kutiev et al.*, 2006]. Second, only part of the observed $N_e(h)$ profile is used in the derivation of the O^+ scale height and the UTH, or equivalently, only an indirect link exists between these parameters and the overall shape of the profile above the F2 peak. Finally, it can be argued that the contribution to the electron density from the protonosphere component is not always negligible at altitudes just above the F2 peak, particularly at local times at night, when the F2 peak of the electron density is typically less marked or even disappears [*Yizengaw et al.*, 2008].

[7] An alternative approach to overcome these limitations would involve separating the contributions to the observed $N_e(h)$ from the ionosphere and the protonosphere components by using different fitting functions for each component [e.g., *Stankov and Jakowski*, 2006], or the same function but allowing different values of the free parameters for each component by, for example, considering the sum of two Chapman or Epstein functions with different scale heights and different densities at the F2 peak [e.g., *Sibanda and McKinnell*, 2011; *Stankov et al.*, 2011]. However, one inconvenience of this last method is that the altitude for the maximum density of each component must be fixed in some way. The usual choice being the assumption that both components reach a maximum at the altitude of the F2 layer peak, h_{mF2}, which seems practical, but it is unclear whether it has any physical justification. Additionally, model functions of this kind are more complicated to work with, since they introduce a larger number of parameters to adjust. It is not unusual to simplify them by reducing the number of free parameters, especially the ones describing the protonosphere component, for example, assuming that some parameters have a typical value or using additional information from other sources to fix them [*Stankov and Jakowski*, 2006; *Sibanda and McKinnell*, 2011; *Stankov et al.*, 2011]. Another important weakness particularly affecting the use of Chapman and Epstein functions is that they rely on a characteristic scale height that is different from the VSH, particularly for altitudes close to h_{mF2}. Although both scale height parameters seem to be clearly correlated [*Liu et al.*, 2007b], no model that directly relates the scale height of the Chapman or Epstein functions and the VSH has yet been formulated.

[8] In the present study, a simple two-component model function is proposed in order to describe the RO-retrieved electron density in the TI above the F2 layer peak. The model function is shown to achieve accurate fits to a wide sample of $N_e(h)$ profiles for altitudes greater than 400 km and for an interval of altitudes of 300 km, where the spherical symmetry assumption provides a very precise determination of electron density profiles from RO data. Using these accurate fits, it is shown that the model provides a quantitative description of the distinct contributions to the observed $N_e(h)$ arising from the ionosphere and the protonosphere components. Several types of evidence are presented to justify the physical validity of the proposed model by means of the best fit parameters and the values of the VSH and the UTH directly inferred from the model. In particular, the correlation between the O^+ scale height and the UTH is shown to be consistent with the results obtained by *Kutiev and Marinov* [2007] using a completely different data sample and methodology.

[9] The structure of the paper is as follows. Section 2 presents and describes the proposed model for the TI, the simplified topside ionosphere plus protonosphere (STIP) model. Section 3 explains the process followed to build the data sample of vertical electron density profiles from CF3 observations. Specifically, this section analyzes the contribution to the slant total electron content (STEC) from ionospheric layers above the LEO satellite and how this contribution can affect RO-retrieved electron density profiles and the subsequent fits by the model function proposed. Section 4 is devoted to validating the performance of the STIP model function when fitting the sample of profiles derived in section 3. To this end, several other function types, namely exponential, α-Chapman, and Epstein are also used to fit the same data set and the fitting results obtained with all the models are compared. In section 5, the model predictions of the UTH and the contribution of the protonosphere to the TI electron density are analyzed and, in particular, the correlation between the O^+ scale height and the UTH directly derived from the fits to the STIP model is investigated. Finally, our conclusions are summarized in section 6.

2. The STIP Model

[10] In order to model RO-retrieved electron density profiles in the TI, taking into account the contribution from the protonosphere, the following function is considered:

$$N_e(h) = N_{O^+}(h) + N_{H^+}(h) = A \exp(-h/H_s) + B, \quad (1)$$

hereafter referred to as the STIP model, where $N_{O^+}(h) = A \exp(-h/H_s)$ and $N_{H^+}(h) = B$ represent, respectively, the densities in the TI of the two major constituent ions O^+ and H^+.

[11] The STIP model has three parameters: A, H_s, and B. The parameter A measures the relative importance of the ionosphere versus the protonosphere component, while it is evident that H_s corresponds to the vertical scale height

associated with the ionosphere (O^+) component. Several studies have found that an exponential function (assuming only one component for the TI) gives a reasonably good fit to the observed electron density profiles in a restricted range of altitudes from $h-h_{mF2}$ greater than 30 or 40 km to the altitude at which the gradient of the observed $\ln N_e(h)$ exceeds its lowest value by 30% [e.g., *Kutiev and Marinov*, 2007]. This justifies, as a first approximation, H_s being considered constant at least in that altitude range. Even if a variable scale height is used to fit electron density profiles, a slow variation for that scale height is typically found [e.g., *Kutiev et al.*, 2006; *Reinisch et al.*, 2007; *Liu et al.*, 2007b, 2008].

[12] The parameter B represents the contribution of the protonosphere (H^+) component to the electron density in the TI region. For altitudes greater than h_{mF2} and assuming that the observed H^+ density has reached its maximum value, the $N_{H^+}(h)$ profile is usually described by a decaying exponential function with a typical scale height of a few thousands of kilometers. Then for a variation of the altitude of about 300 km in a region well above the F2 peak altitude (for example, for an altitude greater than 400 km), one can estimate a variation of the H^+ density which will not be greater than 10–15 %. Consequently, the altitude gradient of the H^+ density is expected to be very small. This justifies, as a first approximation, the protonosphere component in the TI being represented by a constant.

[13] Note that the charge-exchange reaction between the ions H^+ and O^+ (which will not affect the electron density derived from the RO data) might cause a deviation of the best fit exponential term in equation (1) from the true O^+ density and also a deviation of the best fit value of B from the true H^+ density. However, due to the very different scale heights of the two ions, these deviations in the ion composition will only be really significant in a quite reduced range of altitudes.

[14] The simplifications introduced in the STIP model will be subsequently justified by the accuracy achieved in the best fits to the observed $N_e(h)$ profiles for altitudes ranging from 400 km to typically more than 700 km as will be shown in section 4. Moreover, the analysis of the best fit parameters obtained with the STIP model that will be performed in sections 4 and 5 will justify that these parameters really provide a good description of the density of H^+ and O^+ in the range of altitudes of the TI considered in the present work.

[15] On the other hand, from a mathematical point of view, equation (1) is a simplification of the so-called topside ionosphere and plasmasphere model function introduced by *Stankov and Jakowski* [2006] as an adaptive functionality to assist the inversion process leading to the derivation of the observed $N_e(h)$, which in that work was based on data provided by the CHAMP satellite. As pointed out by *Stankov and Jakowski* [2006], the orbit of the CHAMP satellite had a low altitude (nearly 400 km) and the contribution from the ionosphere above that LEO satellite could not be ignored in order to determine the upper boundary condition required by the classical inversion process. To this end, the authors assumed that for altitudes above the CHAMP orbit, the electron density was given by the sum of an α-Chapman function and an exponential term. This model function was applied up to altitudes of several thousands of kilometers just in order to achieve a smooth transition between the values of the density provided by the model and the densities computed from RO data. However, in the present work, equation (1) is intended to model the TI region, specifically for altitudes from several tens of kilometers above the F2 layer peak to the typical altitude of the CF3 satellites (about 800 km), which is several hundreds of kilometers higher than the altitude of the CHAMP satellite.

[16] Let us consider the derivation from the STIP model of some basic parameters characterizing the TI and the ionosphere/plasmasphere interplay. In accordance with its conventional definition, the ionosphere UTH can be obtained from equation (1) by finding the altitude at which $N_{O^+}(h)$ equals $N_{H^+}(h)$. Denoting that altitude as H_u one obtains

$$H_u = H_s \ln\left(\frac{A}{B}\right) . \tag{2}$$

Then, isolating B from equation (2) and substituting into equation (1), one can derive an expression for the altitude dependence of the VSH that is associated with the electron density gradient,

$$\mathrm{VSH} \equiv -\left(\frac{\mathrm{d}\ln N_e(h)}{\mathrm{d}h}\right)^{-1} = H_s\left[1+\exp\left(-\frac{H_u-h}{H_s}\right)\right] . \tag{3}$$

From equation (3), one can see that the VSH predicted by the STIP model grows as a function of altitude, h, taking a minimum value $\mathrm{VSH} \simeq H_s$ when $H_u - h \gg H_s$. Specifically, for altitudes near the typical values of h_{mF2}, one expects that the VSH will deviate only a few percent from H_s, which supports the empirical approach introduced by *Kutiev et al.* [2006] and subsequently used in other studies to derive the scale height of the O^+ component. On the other hand, as h approaches the value of H_u, the VSH becomes approximately $2H_s$.

[17] On the other hand, a conventional method to estimate the local value of the VSH involves selecting two values of the observed $N_e(h)$ profile at two altitudes, h_0 and $h_0 + \Delta h$, and then approximating the derivative in equation (3) by the ratio between differences. This leads to

$$\mathrm{VSH} = \Delta h\left\{\ln\left[\frac{N_e(h_0)}{N_e(h_0+\Delta h)}\right]\right\}^{-1} , \tag{4}$$

where the altitude h_0 is chosen at least a few tens of kilometers above the F2 layer peak, while Δh must be greater than 20–30 km to prevent a noisy derivation of the VSH. In section 5, the STIP model prediction provided by equation (3) will be compared with the empirical derivation of the VSH obtained with equation (4).

[18] An empirical derivation of the O^+ scale height can also be performed in the following way. Assume that the STIP model function is a good approximation to an observed $N_e(h)$ profile for some unknown values of the three parameters A, H_s, and B. Then, selecting three values of $N_e(h)$ at altitudes h_0, $h_0 + \Delta h$, and $h_0 + 2\Delta h$ and fitting equation (1) to such values at the respective altitudes leads to a system of three equations. After solving the system, an empirical estimate of the scale height H_s is obtained as

$$H_s = \Delta h\left\{\ln\left[\frac{N_e(h_0)-N_e(h_0+\Delta h)}{N_e(h_0+\Delta h)-N_e(h_0+2\Delta h)}\right]\right\}^{-1} , \tag{5}$$

where the same restrictions as mentioned after equation (4) concerning the altitude h_0 and the interval Δh must also be applied in this case.

3. The Data Sample Derivation

[19] The data collected for the present investigation were measurements of GPS signals taken during RO by satellites from the CF3 constellation, which is composed by six LEO satellites, five of them with altitudes between 740 and 860 km. The RO measurements correspond to 12 complete days during 2009, separated by intervals of 30 days (i.e., 1 day per month). For that year, almost the full set of CF3 satellites was deployed meaning that a large quantity of RO data were available. The measurements have been processed to derive the values of the difference between the L1 and L2 GPS carrier phases (the ionospheric combination $L_I = L_1 - L_2$) during occultation events. Occultations were initially selected when the measured impact parameters of the different GPS-LEO rays (that is, the radial distance from the Earth center to the GPS-LEO straight line), observed with negative elevations, covered a corresponding interval of altitudes over the Earth's ellipsoid that included the range between 200 and 700 km.

[20] For every selected occultation, the vertical profile of the electron density was calculated (see below for details), yielding an initial set of nearly 14,300 profiles. From this set, those cases showing unrealistic negative densities at altitudes between 400 to 700 km were removed. In addition, profiles with an F2 peak at an altitude greater than 350 km were excluded in order to focus the study clearly in the TI (see section 4 for details). A final set was obtained containing 13,740 profiles (i.e., 96% of those from the initial set) which sparsely samples the ionosphere electron density during 2009 for different seasons of the year, local times, and latitudes. In that way, the data set covered a wide range of physical conditions of the TI sufficient for checking the STIP model predictions as well as for comparing its performance with other model functions commonly used in the literature.

[21] Concerning the derivation of the $N_e(h)$ profiles, the procedure described in *Hernández-Pajares et al.* [2000] has been applied with the exception that spherical symmetry is assumed since our interest is focused on the TI. Note that the *Hernández-Pajares et al.* [2000] methodology can be applied to any LEO satellite, and it is not specific for CF3 satellites. For this reason, in the rest of the paper, we will refer to a LEO satellite in general, and when the results apply only to CF3 satellites, this will be specifically indicated. Following *Hernández-Pajares et al.* [2000], the equation that relates the STEC to the observed values of L_I is inverted for a set of GPS-LEO rays of impact parameter, p_i, $i = 1, \ldots, M_{\text{obs}}$, with M_{obs} being the number of observations with negative elevation during a single occultation event:

$$L_I(p_i) = 2\alpha \sum_{j=1}^{i} N_e(p_j) l_{ji} + \alpha \text{STEC}_A + b\,, \tag{6}$$

where $\alpha = 0.105$ m TECU^{-1}, STEC_A is the contribution to the STEC from the ionosphere shells above the LEO satellite, b is the carrier phase ambiguity of L_I, $N_e(p_j)$ is the electron density in a spherical shell enclosing the impact parameter, p_j, and l_{ji} is the path length of the ith GPS-LEO ray across the jth shell below the LEO satellite, the usual onion-skin model geometry being assumed, with $i = 1$ corresponding to the uppermost shell (see more details of the inversion model geometry in *Hernández-Pajares et al.* [2000, Figure 1]).

[22] Subtracting a reference measurement, $L_I(R) = \text{STEC}_R + b$, from equation (6) allows the carrier phase ambiguity term to be canceled out. Finally, choosing $L_I(R)$ such that $\text{STEC}_A \approx \text{STEC}_R$ (for example, taking $L_I(R)$ equal to the first measurement just above the occultation horizon), the contribution from the ionosphere above the LEO satellite can be considered negligible. In this way, the derivation of the values of $N_e(p_j)$ from L_I measurements can be performed by simply inverting the following triangular system of equations:

$$\alpha^{-1} [L_I(p_i) - L_I(R)] = 2 \sum_{j=1}^{i} N_e(p_j) l_{ji}\,, \quad i = 1 \ldots, M_{\text{obs}}\,. \tag{7}$$

[23] When applying the aforementioned methodology, it is important to address the effects in the estimation of the electron density profile arising from, first, the validity of the spherical symmetry assumption and, second, the possible difference between the values of STEC_A and STEC_R, which would lead to a mismodeling of the ionospheric delays produced above the LEO orbit.

[24] Taking into account the geometry of a typical RO, the effects of nonspherical features in the ionosphere are clearly less relevant as the altitudes considered increase. The path length of a GPS-LEO ray across the ionosphere below a LEO satellite decreases as the impact parameter of the ray increases. For example, this length typically decreases by more than a factor of two when the altitude corresponding to the impact parameter of the ray increases from 100 to 400 km. Therefore, significantly smaller errors are expected when one assumes spherical symmetry for the TI than for the bottom-side ionosphere. As pointed out earlier, the STIP model focuses on the TI region, specifically, altitudes larger than 400 km and only cases for which the F2 peak is below 350 km will be considered to fit the $N_e(h)$ profiles (see details in section 4). Thus, the use of spherical symmetry is very suitable for our purposes, and it is not necessary to apply the improved inversion algorithm introduced by *Hernández-Pajares et al.* [2000] for the electron density retrieval.

[25] On the other hand, setting STEC_A equal to STEC_R is equivalent to assuming that the electron density profile above the LEO satellite is essentially zero during the occultation. Hence, one can address the effects in the retrieved profile of a difference between these two quantities by considering a nonzero electron density above the LEO orbit.

[26] Figure 1 shows the vertical electron density profiles retrieved by means of equation (7) using the values of L_I calculated from several simulated occultations and taking $L_I(R)$ equal to the corresponding value of L_I at the LEO orbital radius. To generate the L_I measurements of the simulated occultation, the electron density profile was assumed to be given by a Gaussian function. For the geometry of the simulated occultation, the actual rays corresponding to a real occultation with the typical orbital radii of CF3 and GPS satellites were used to evaluate the STEC and, subsequently, to derive the corresponding L_I measurements. In the three simulations shown in Figure 1, the altitude of the peak of the Gaussian electron density was set equal to 330, 1030, and 1630 km, respectively, while the altitude of the LEO satellite

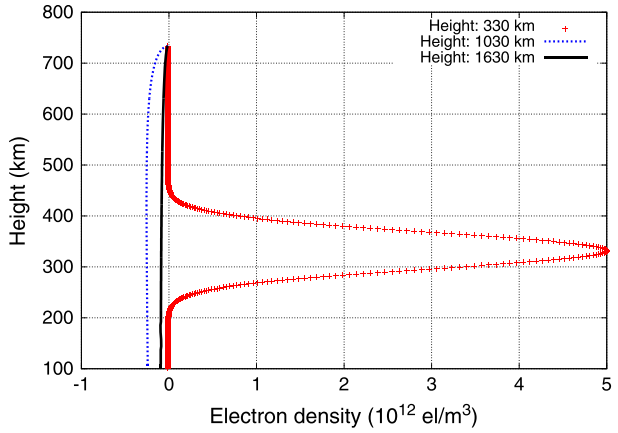

Figure 1. The vertical electron density profile retrieved from a simulated RO with the STEC measurements derived from a Gaussian-shape electron distribution above or below an LEO satellite orbiting at an altitude similar to a CF3 satellite. See the legend in the top-right corner of the plot for the different altitudes considered for the Gaussian peak.

was set equal to nearly 730 km in all the cases. The magnitude of the maximum density was set to $5 \cdot 10^{12}$ el/m^3, which is similar to the greatest values measured at the F2 layer peak in observed $N_e(h)$ profiles.

[27] As expected, the inversion of the profile by means of equation (7) when the altitude of the Gaussian peak is 330 km (below the altitude of the LEO satellite) yields essentially the same density profile as that initially considered (crosses in Figure 1). However, this is not the case when the Gaussian peak is placed at altitudes above the LEO satellite (dotted and solid curves in Figure 1). The quantitative effect of an electron density concentrated above the LEO satellite on the retrieved $N_e(h)$ profile below the LEO satellite is essentially equivalent to a constant negative bias, except at altitudes just below the LEO satellite.

[28] The magnitude of the bias is nearly two orders of magnitude smaller than the peak value of the profile when the altitude of the peak is 1030 km, a few hundred kilometers above the LEO altitude, and the magnitude of the bias decreases as the altitude of the Gaussian peak increases. Thus, taking into account the typical expected values for the true electron density above the LEO satellite (which should be several orders of magnitude lower than $5 \cdot 10^{12}$ el/m^3, the value assumed for the peak of the simulated profile), one can conclude that the mismodeling resulting from a difference between STEC$_A$ and STEC$_R$ will be negligible, provided that a reasonable value of $L_I(R)$ has been used to retrieve the profile. The constant negative bias in the retrieved profile will be essentially absorbed into the value of the constant B when fitting the model function (1) to an observed $N_e(h)$ profile. Nevertheless, the magnitude of such bias will usually be irrelevant compared to the values for the density of the protonosphere component in the TI (see section 5 and Figure 8).

[29] Going one step further, one can also analyze the effects on the shape of the retrieved $N_e(h)$ profile when considering different (although well justified) values for the reference measurement, $L_I(R)$, subtracted in equation (7). To this end, we have computed the differences between the two $N_e(h)$ profiles obtained from using two different values of $L_I(R)$ for the same occultation. For this comparison, we use our sample of occultations extracted from CF3 measurements as described at the beginning of this section. In one case, $L_I(R)$ was set equal to the minimum value of L_I measured during the occultation for negative elevations plus a typical measurement noise of 0.01 m. In the other case, $L_I(R)$ was calculated averaging the 10 L_I measurements for positive elevations just above the occultation horizon. Figure 2 shows the root-mean-square (RMS) differences between the two profiles at different altitudes obtained from our sample of occultations. One can observe that the RMS difference is nearly $5 \cdot 10^8$ el/m^3 when the altitude considered is close to 10 km below the maximum altitude reached by the $N_e(h)$ profiles (normally the altitude of the LEO satellite). The RMS difference keeps on decreasing as one descends in altitude, and remains several orders of magnitude smaller than the typical values found for $N_e(h)$ at the corresponding altitude. Consequently, the effect of the two different choices considered for $L_I(R)$ in the resulting density profile is usually negligible for altitudes which are separated more than nearly 10 km from the maximum altitude for which the electron density profile has been computed.

[30] To summarize, it can be concluded from the analysis described above that the impact of a mismodeling of the STEC$_A$ in the electron density profiles retrieved from RO for altitudes below the LEO satellite will typically be negligible. The same conclusion applies to the specific value chosen for $L_I(R)$ in order to cancel out the bias term and the STEC$_A$, even if that value does not coincide with the observed L_I at zero elevation, the stronger effects are limited at altitudes just below the altitude of the LEO satellite. These results imply that the methodology described in this section, to calculate the electron density using RO measurements from a LEO satellite of the CF3 constellation, is essentially sensitive to the electron distribution below the LEO satellite, the

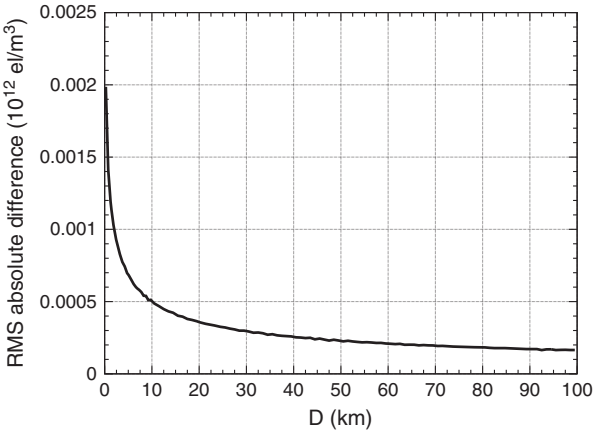

Figure 2. Comparison of the differences between the two $N_e(h)$ profiles obtained using the two different values for $L_I(R)$ considered in section 3. The curve corresponds to the RMS absolute difference (drawn from the sample of profiles considered in this work) between the two determinations of $N_e(h)$ as a function of $D = h_{\mathrm{LEO}} - h$, the vertical distance from a given altitude h to the maximum altitude h_{LEO} reached by the profile, normally equal to the altitude of the LEO satellite.

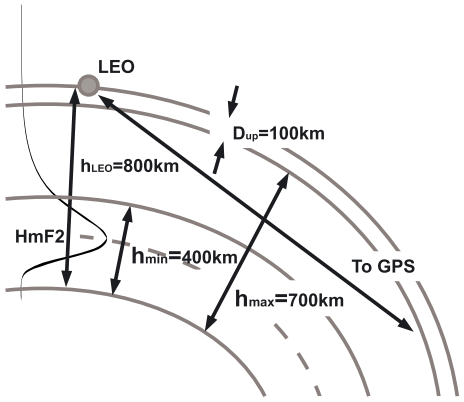

Figure 3. Layout of the altitude range used to perform the fits to the observed electron density profile in the particular case that the RO measurements were obtained by a LEO satellite at an altitude of 800 km.

effects of the electron content above the LEO satellite being almost negligible in the density profile finally obtained. Note that this conclusion not only concerns CF3 satellites in particular, but can also be applied to other LEO satellites at a similar altitude.

4. Electron Density Profile Fitting in the Topside Ionosphere

[31] In order to validate the performance of the STIP model compared to that of one-component models, another three functions in addition to equation (1) were considered to fit the sample of electron density profiles described in section 3. An exponential function,

$$N_e(h) = N_0 \exp(-h/H_0)\,, \tag{8}$$

an α-Chapman function,

$$N_e(h) = N_0 \exp\{0.5[1 - z - \exp(-z)]\}\,, \tag{9}$$

and an Epstein function,

$$N_e(h) = N_0 \,\mathrm{sech}^2(z/2)\,, \tag{10}$$

where $z = (h - h_{mF2})/H_0$, with H_0 representing the scale height of the corresponding profile, assumed to be independent of altitude, and h_{mF2} is the altitude of the F2 layer peak. The free parameters considered for the functions (8) to (10) are just N_0 and H_0, whereas for the STIP model, the three parameters to be adjusted are A, H_s, and B. Note that the Chapman and the Epstein functions have a maximum at an altitude of h_{mF2}, and this will be determined from the maximum of the observed electron density profile. Consequently, h_{mF2} is not considered a free parameter to adjust in the present study. Further, note that in the case of equation (8), the scale height H_0 coincides with the usual definition of the VSH as $-\mathrm{d}h/\mathrm{d}\ln N_e(h)$, whereas for the STIP model, the scale height H_s corresponds to the same derivative but for the density of O^+ (the ionosphere component). In contrast, for the Chapman and Epstein functions, the VSH is nearly $2H_0$ only when $h - h_{mF2} >> H_0$.

[32] Every $N_e(h)$ profile in our sample (containing 13,740 profiles) has been fitted to each model function considered for a range of altitudes from a constant minimum value, h_{min}, up to a maximum altitude, $h_{max} = h_{LEO} - D_{up}$, normally depending on the altitude over the Earth's ellipsoid of the particular CF3 satellite, h_{LEO}. In a few occultations, the observations did not reach to the CF3 satellite altitude, and in these cases h_{LEO} was substituted by the uppermost altitude reached by the RO measurements with negative elevation. For all the profiles h_{min} was set equal to 400 km. This value was chosen to achieve a compromise between covering, on the one hand, the altitudes of interest for our study, namely, the TI and lower plasmasphere and, on the other, avoiding the influence of the F2 layer peak. In relation to this, as mentioned in section 3, all profiles with a maximum at altitudes greater than 350 km were previously excluded from our sample. As for the value of h_{LEO}, it may range approximately between 740 km and 860 km depending on the orbit of the particular CF3 satellite, although h_{LEO} is typically greater than 800 km. Finally, a value of $D_{up} = 100$ km has been chosen for all the profiles or our sample in order to exclude altitudes near the CF3 satellite from the fits, in this way,

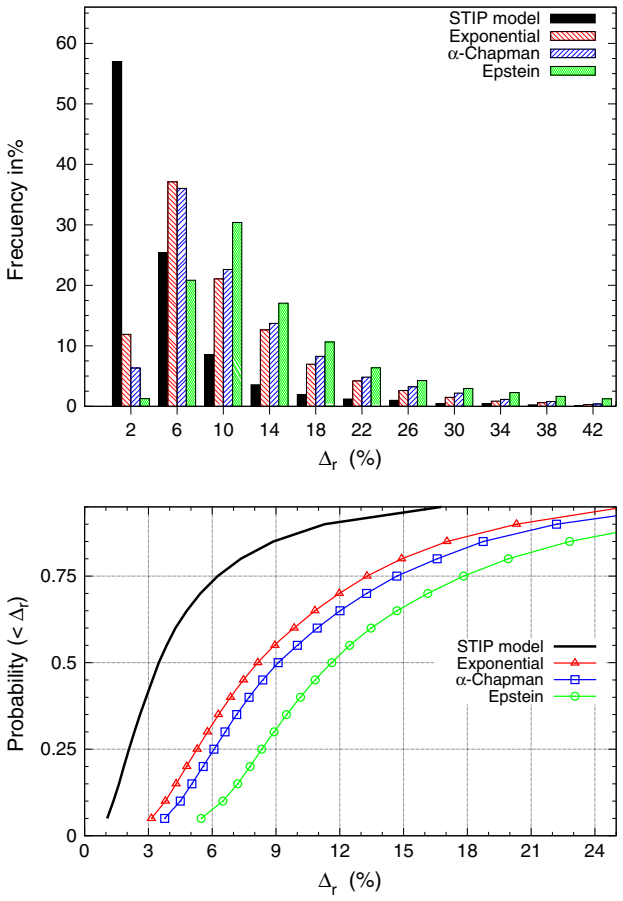

Figure 4. Histogram of the frequency distribution (top) of mean relative differences, Δ_r, obtained for the different fitting functions analyzed. Each label in the horizontal axis corresponds to the central value of the bin used for the four histogram bars over the label. Each group of four bars has been obtained using a constant bin-size of 4. Cumulative distribution function (bottom) of the Δ_r values obtained from the fits to the sample of profiles analyzed with the four fitting functions considered.

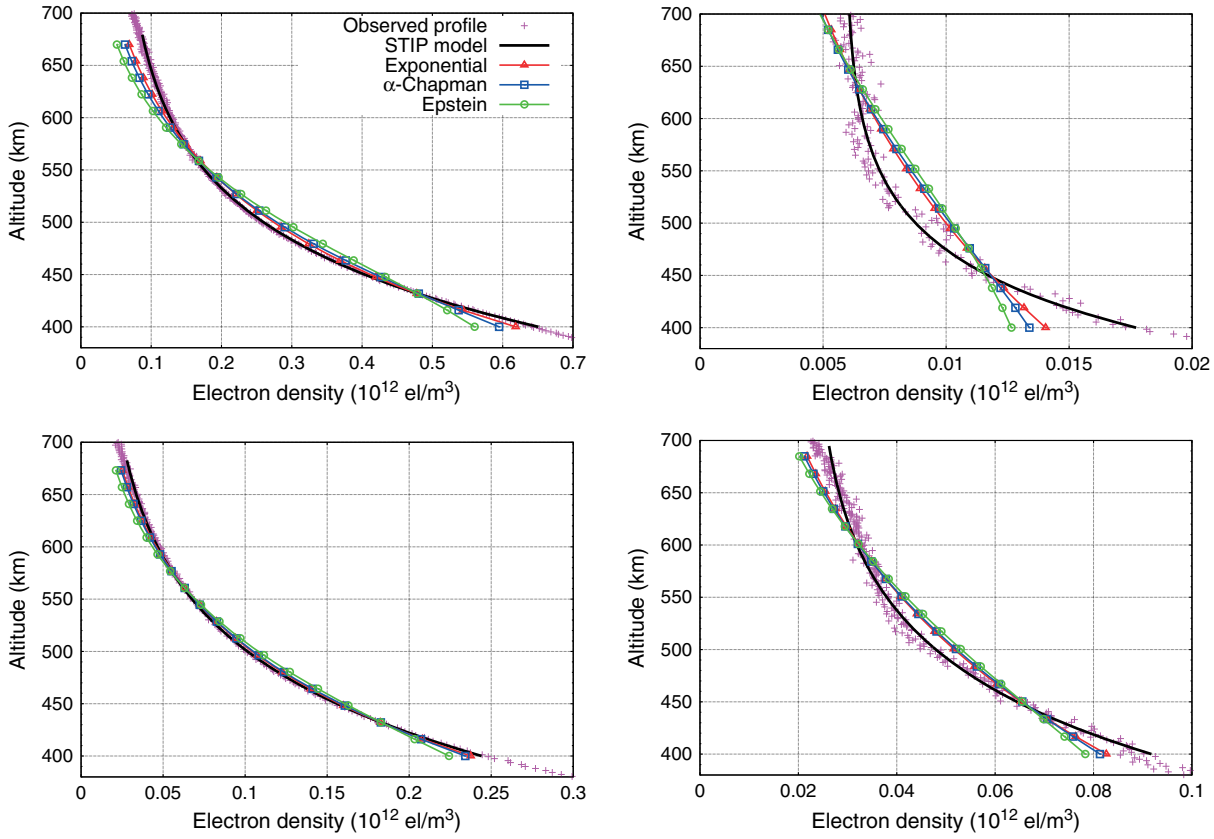

Figure 5. Some examples of observed $N_e(h)$ profiles (crosses) and the corresponding best fit curves (see legend in the top-left panel) obtained with the four model functions considered in this work and shown only for the range of altitudes used in the fits. These four occultations were selected during day 328 of 2009 at different local times (LT) and geographic latitudes (LAT). (top left) [LT, LAT] = [15.5 h, –16°]; (top right) [LT, LAT] = [2.8 h, 24°]; (bottom left) [LT, LAT] = [13.7 h, –46°]; and (bottom right) [LT, LAT] = [18.8 h, –55°]. The observed profiles in Figures 5 (top and bottom) were derived, respectively, from carrier phase measurements of GPS satellites-PRN 2 and 3.

eliminating the possible effects on the profiles described in section 3 due to a mismodeling of the ionosphere above the CF3 satellite. For that purpose, the value selected for the parameter D_{up} is more than sufficient and the resulting values of $h_{\max}$ were greater than 700 km in 55% of the profiles fitted, while $h_{\max} > 600$ km for all the fits performed. Further, note that the present study focuses in a range of altitudes for which the RO-retrieved electron density profiles are particularly reliable. Figure 3 illustrates schematically the range of altitudes used for the fits in the particular case of a LEO satellite with an altitude equal to 800 km.

[33] In order to compare the performance of the best fits obtained with the four model functions under consideration, we evaluated the average of the absolute value of the relative difference between the observed electron density profile and each best fit profile,

$$\Delta_r = \frac{1}{M}\sum_{i=1}^{M}\left|1-\frac{N_e^{(\mathrm{obs})}(h_i)}{N_e^{(\mathrm{fit})}(h_i)}\right|, \qquad (11)$$

obtained after applying the Levenberg-Marquardt method to perform a nonlinear least squares fitting, where h_i, $i = 1, \ldots M$, are the altitudes within the fitting range $[h_{\min}, h_{\max}]$ for which the values of the observational profile were calculated according to equation (7). Note that the same fitting interval is used for all the model functions.

[34] After obtaining the best fit parameters, several cases were excluded from the subsequent analysis. Specifically, those giving an extremely poor fit with values of Δ_r exceeding 50% were removed, as were any with best fit parameters which were physically meaningful, for example, those with negative best fit values of N_0, A, or B and extremely large values of H_s or H_0 (greater than 900 km). The cases excluded represented between 3 and 6% of the initial sample of density profiles fitted, depending on the model function considered.

[35] Figure 4 (top) displays the histogram of the distribution of Δ_r values (in %) obtained for the different model functions analyzed. Figure 4 (bottom) shows the corresponding cumulative distribution function (CDF) of Δ_r. It can be seen clearly that the best results are achieved with the STIP model. In particular, Figure 4 (top) shows that nearly 57% of the cases in our sample have a mean relative difference between the best fit and data smaller than 4% for the STIP model, while for the rest of models considered, the best case is the exponential model with which $\Delta_r < 4\%$ for only nearly 12% of cases. From a statistical point of view, one can see from Figure 4 (bottom) that the median

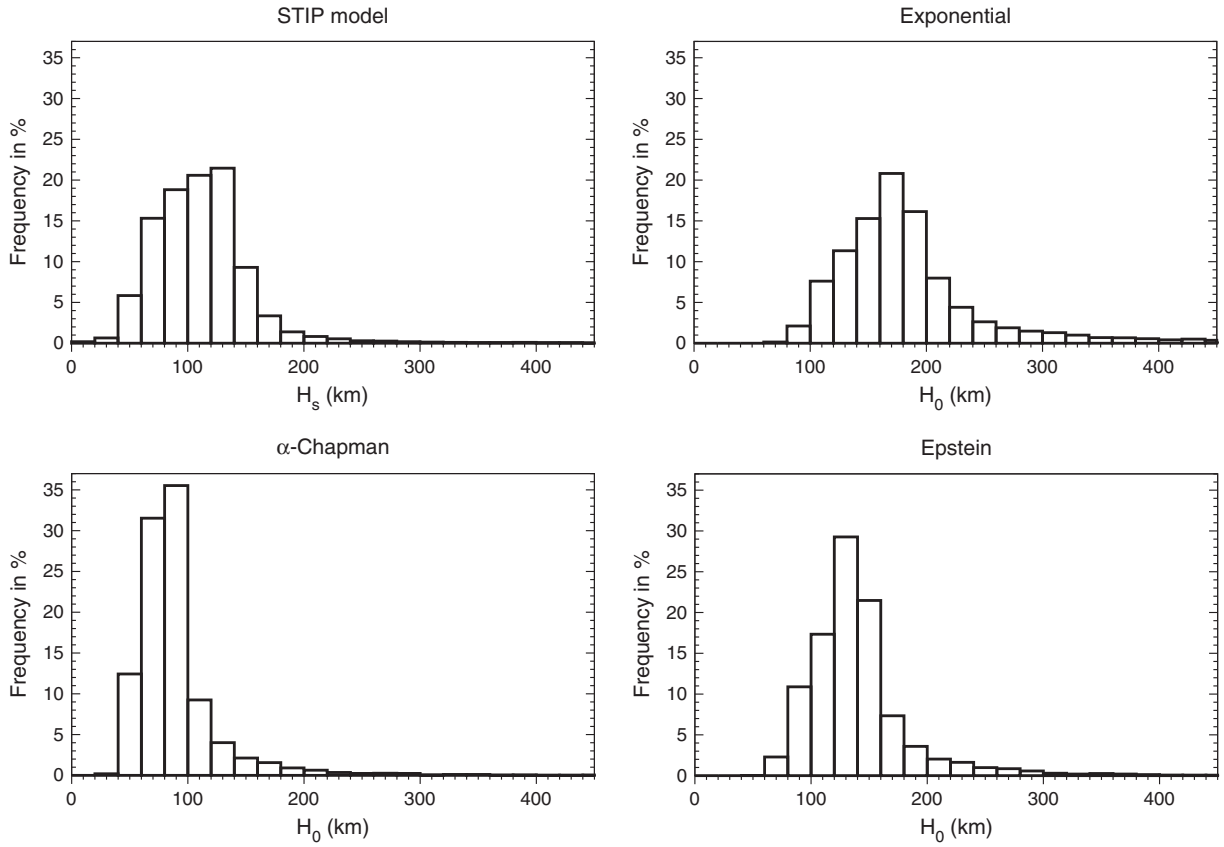

Figure 6. Frequency distribution of the scale heights obtained from the fits with the STIP model (top left), the exponential function (top right), the α-Chapman function (bottom left), and the Epstein function (bottom right).

of the Δ_r distribution is 3.5% for the STIP model, while for the rest of functions, it is greater than 8% and, in general, the probability of achieving a fit to an observed $N_e(h)$ in our sample with a resulting Δ_r value below a fixed threshold is always substantially larger with the STIP model than with the rest of the model functions considered.

[36] Hence, it can be concluded that the STIP model function not only achieves a good fit for most of the profiles in the sample, but also significantly better fits than in the case of the other classical model functions, with more than a factor of two reduction in Δ_r, at least in the fitting range of altitudes analyzed. Figure 5 illustrates this conclusion for a few specific cases, showing some examples of best fit curves compared to the corresponding observed $N_e(h)$ profile fitted.

[37] A comparison of the distribution of the scale height values derived after the best fits with the four model functions considered is presented in Figure 6. These graphs demonstrate that there is a significant difference between the typical O^+ scale height, H_s, inferred from the STIP model, which has a median value of nearly 100 km, and the VSH that would be inferred with single-component models of the TI. Recall that for the exponential function, the values of H_0 shown in the histogram of Figure 6 correspond to the VSH, while for the Chapman and Epstein functions, the VSH will instead be equal to $2H_0$ if such models were approximated by an exponential function in order to derive the VSH. Hence, for the one-component models considered in this study, the median value of the VSH is nearly 200 km, a factor of 2 larger than the O^+ scale height found with the STIP model. This is in agreement with equation (3) that predicts a similar trend for the VSH as the altitude increases and approaches the value of the UTH.

[38] Figure 7 (top) shows an example of the comparison between the STIP model prediction from equation (3) for the altitude variation of the VSH and the corresponding empirical values obtained directly from the observed $N_e(h)$ profile using equation (4). A cubic spline interpolation of the observed profile was calculated before using this latter equation in order to reduce the noise of the empirical VSH determination. One can see that for the altitudes across the fitting range (solid curve), there is a good agreement between the predicted and the empirically calculated VSH. This feature is characteristic of most of the profiles in our sample, for which the VSH predicted by the model is fully consistent with the corresponding values directly obtained from the observed profiles for altitudes in the TI.

[39] Moreover, consider reproducing an observed $N_e(h)$ profile by means of an α-Chapman function but replacing N_0 and H_0 in equation (9) with the best fit values of A and H_s, respectively, obtained with the STIP model. Then, add to that new function the best fit value of B also obtained with the STIP model and, finally, set h_{mF2} equal to the true peak altitude of the observed profile. The resulting profile and the corresponding observational profile are compared in Figure 7 (bottom), where it can be seen that they closely match for the altitude range used for fitting the observed

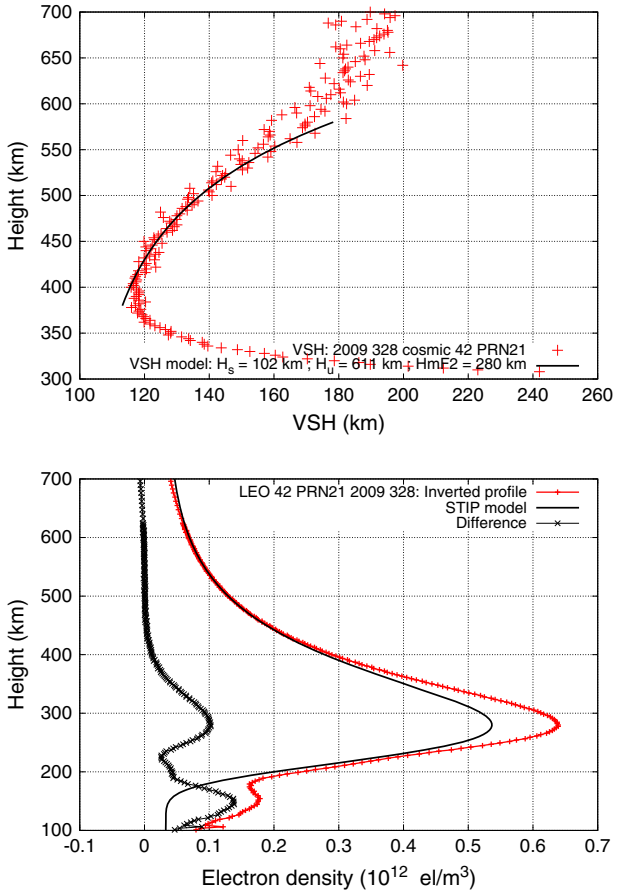

Figure 7. Top: The STIP model prediction (solid line) for the VSH calculated with equation (3) compared with the corresponding empirical determination (crosses) of the VSH obtained from an observed profile using equation (4). Bottom: The adjusted α-Chapman profile (solid line) using the parameters obtained with the STIP model compared with the corresponding observational profile and the difference between the two profiles.

profile. On the other hand, for altitudes below 400 km, there are differences between the two, as expected, since for these altitudes, the observed profile can be affected by the use of the spherical symmetry assumption as well as by the existence of ion species other than O^+ and H^+, particularly for altitudes near to and below the F2 peak. Hence, Figure 7 illustrates that, despite its apparent simplicity, the STIP model provides a set of parameters that are able to accurately reproduce the observed electron density profile in the TI region. At the same time, for altitudes around h_{mF2} and lower, the STIP model parameters provide a reliable reference that could subsequently be used (once the effects of non-spherical symmetry had been properly calibrated) to quantify the contribution to the ionospheric composition arising from ion constituents other than O^+ and H^+.

5. STIP Model Predictions for the UTH and the Protonosphere Contribution to the TI

[40] An important conclusion inferred from the results presented in section 4 is that the observed electron density profile in the TI can generally be explained by the coexistence of two main types of ions, O^+ and H^+, so that the contribution of the protonosphere component to the total electron content (represented by the best fit values of B) cannot be ignored. Moreover, the good fits achieved by the STIP model with constant values of both the scale height, H_s, and the density of the protonosphere component, B, imply that the two components of the TI are essentially isothermal, at least in the fitting range analyzed.

[41] On the other hand, the altitude dependence of the VSH predicted by the STIP model traces the altitude variation of the plasma temperature in the TI region. That variation is a consequence of changes in the ratio between abundances of each TI component with altitude, changes in these abundances being caused by the density of the O^+ component decreasing more rapidly with altitude than the H^+ component.

[42] In order to achieve a reliable derivation of the VSH and the UTH by means of the STIP model, the best fit values of B must provide a good characterization of the density of the protonosphere component. Thus, for the subsequent studies performed in this section, only those best fits to the STIP model with $\Delta_r < 10\%$ will be considered, which are nearly 88% of the cases from the initial sample. By means

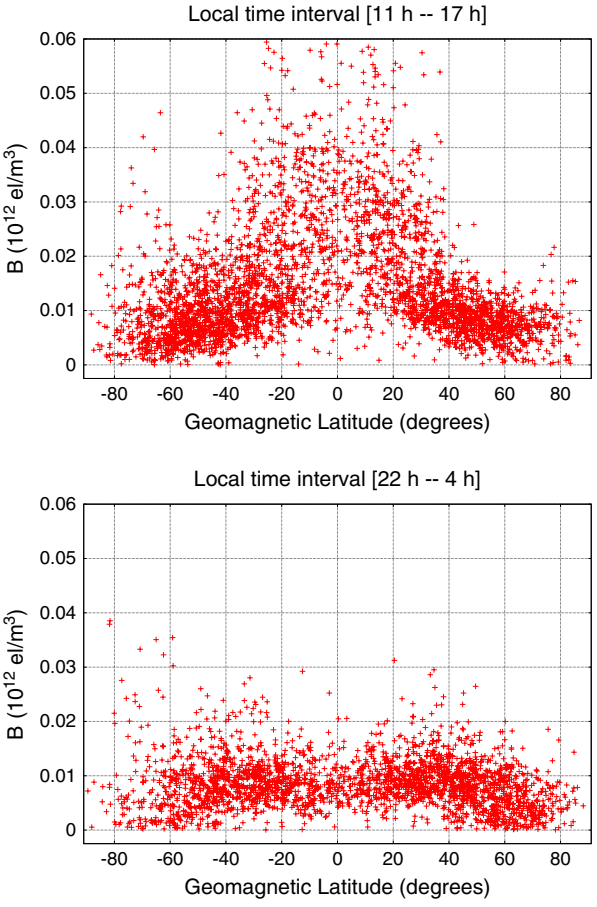

Figure 8. Distribution of best fit values of B from the STIP model as a function of geomagnetic latitude for local times around midday (top) and around midnight (bottom). Only data from fits with $\Delta_r < 10\%$ are shown.

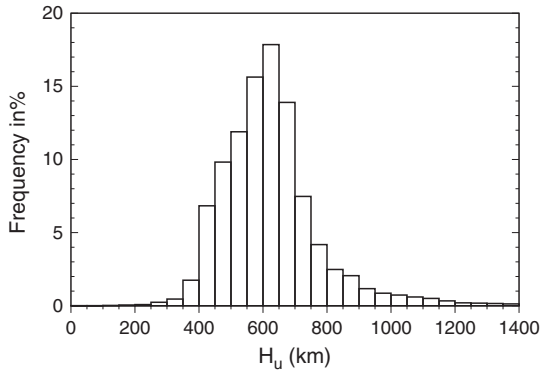

Figure 9. Histogram of the frequency distribution of the UTH during 2009 from the sample of electron density profiles considered in this study.

of this choice, we intend to exclude from the sample the majority of cases for which the assumption of a constant H^+ density might not be a good approximation for the true distribution of the protonosphere component.

[43] For the sample of profiles selected, Figure 8 represents the best fit values of B as a function of geomagnetic latitude for two different local time intervals, between 11 and 17 h and between 22 and 4 h. It is evident from Figure 8 that, particularly for local times around midday, the values of B are significantly larger near the geomagnetic equator and decrease toward the geomagnetic poles, while during the night, the magnitude of this component is very similar at all geomagnetic latitudes. These are the same trends as expected for the ion density in the protonosphere [*Yizengaw et al.*, 2008]. The range of best fit values of B is also in quantitative agreement with the typical values of the vertical total electron content contributed by the protonosphere, TEC_p. Indeed, let us assume an exponential decay of the H^+ ion density with altitude with a scale height of a few thousands of kilometers and consider the value for the bottom-side protonosphere density to be represented by the parameter B. Then, integrating over altitudes from the TI to arbitrarily large heights, one would obtain a rough estimate of TEC_p simply as the product of B times the protonosphere scale height. For the range of values of B shown in Figure 8 for low geomagnetic latitudes, this would yield a range of values of TEC_p between 1 and 10 TECU, which is fully consistent with the values typically measured for the total electron content of the protonosphere [e.g., *Yizengaw et al.*, 2008; *Bishop et al.*, 2009; *Mazzella Jr.*, 2009; *Lee et al.*, 2013].

[44] Using the results obtained with the STIP model, one can also investigate the correlation between the scale height of the O^+ component, H_s, and the UTH, H_u. In a previous study, using a database of electron density profiles derived from topside sounders, *Kutiev and Marinov* [2007] found a significant correlation between the scale height of the O^+ population and the UTH for middle geomagnetic latitudes. The procedure used by *Kutiev and Marinov* [2007] to derive the O^+ scale height and the UTH was introduced by *Kutiev et al.* [2006], and it has been briefly described in section 1, fourth paragraph. In this procedure, the altitude range for the derivation of the O^+ scale height (which considers a minimum altitude greater than h_{mF2}) depends on the gradient of the particular electron density profile considered. Hence, both the database and the methodology employed for the present study of the H_s versus H_u correlation are different from those used by *Kutiev and Marinov* [2007].

[45] Figure 9 shows the histogram of the distribution of the H_u values obtained in the present work. Comparing these with the corresponding histogram of *Kutiev and Marinov* [2007, see their Figure 1], the results seem to be completely consistent. Both histograms have a peak around 700 km and show an asymmetric distribution with a long tail for large values of the UTH which have a very low frequency. Also, the range of UTH values covered by both histograms (discarding the lowest frequency values of the tails) is similar. Further, the range of values of the UTH found by *Yue et al.* [2010, see their Figure 4] after analyzing a database of RO measurements from the CF3 constellation during the whole year of 2008 is also consistent with the range of values shown by Figure 9 from our sample covering the year of 2009.

[46] Concerning the values of the O^+ scale height, the histogram of H_s values shown in Figure 6 (top left) seems also consistent with the corresponding histogram presented in *Kutiev and Marinov* [2007, Figure 1]. In both cases, the maximum of the distribution is close to 120 km, while the range of values of the scale height having a frequency greater than 1% goes approximately from 50 km to 250 km.

[47] Figure 10 represents the pairs of values of H_s and H_u for our data set. It also shows the corresponding linear least squares fit to the complete data set and to a subset of data corresponding to the profiles that show the most accurate fits to the STIP model (see figure caption). The slope of the linear best fit obtained in this latter case was equal to 0.18, and the linear correlation coefficient was equal to 0.73, compared with a slope equal to 0.21 and a linear correlation coefficient equal to 0.8 found by *Kutiev and Marinov* [2007]. Although the correlation coefficient is slightly lower for our sample, it is important to note that *Kutiev and Marinov* [2007] examined the correlation for a midgeomagnetic latitude interval, daytime hours, and winter months. In contrast, the results shown in Figure 10 were drawn from

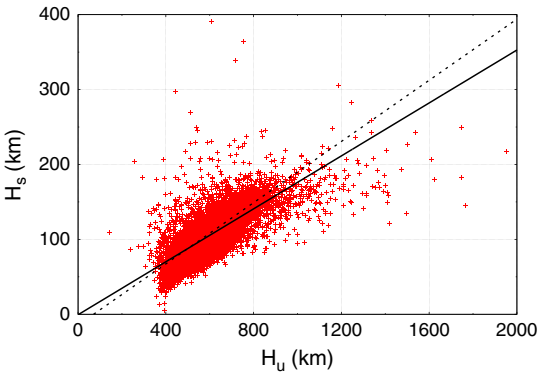

Figure 10. The O^+ scale height, H_s, versus the UTH, H_u, for the STIP model fits with $\Delta_r < 10\%$ (red crosses), and the corresponding linear least squares fit (solid line). The linear least squares fit obtained from the whole sample (without any restriction for Δ_r) is also shown for comparison (dotted line).

a sample without any such restrictions covering all of 2009 and, hence, they clearly suggest that the correlation between the O^+ scale height and the UTH remains significant, regardless of the local time, season and even the geomagnetic latitude considered.

[48] According to the STIP model, the ratio between H_u and H_s is directly related with that of A and B through equation (2). From a physical point of view, a reasonable interpretation of the observed correlation between the O^+ scale height and the UTH is the existence of a correlation between the characteristic-density parameters A and B which measure the respective contribution to the TI of each ion constituent. This is, in fact, confirmed by the analysis of the linear fit to the pairs (A, B) obtained from the STIP model, which yields a linear correlation coefficient of 0.71, very similar to the one obtained for the linear fit shown in Figure 10.

6. Summary and Conclusions

[49] The present work has shown that, by means of a simple approach considering two components representing the density of the O^+ and H^+ ions, the STIP model is able to provide an accurate description of RO-retrieved electron density profiles in the TI region (specifically, in the altitude range going from 400 km up to a maximum altitude between 700 and 800 km). Despite the fact that the STIP model is not intended to reproduce the electron density around the F2 layer peak and despite that the range of altitudes considered for the fits is only part of the whole extension of the TI, the different studies that have been presented in this work support the reliability of the STIP-model results at least for an altitude range of nearly 300 km in the TI.

[50] We have also presented a study demonstrating that for LEO satellites having altitudes similar to those of CF3 satellites, the electron density profiles derived from RO data using the methodology described in section 3 are essentially sensitive to the electron distribution below the LEO satellite. Our results show that the error introduced in the profile by the possible mismodeling of the STEC above the LEO orbit is negligible, the strongest effects being restricted to the first few tens of kilometers below the altitude of the LEO satellite. Thus, in our subsequent analysis, an interval of altitudes of 100 km just below the LEO satellite altitude has not been considered and, consequently, the best fit parameters obtained with the STIP model fits to our sample are mostly unaffected by errors caused by the possible mismodeling of the STEC above the CF3 satellites. This has allowed us to obtain reliable values of the key parameters characterizing the TI, namely the O^+ scale height, the ionosphere UTH, the altitude variation of the VSH, and the density contribution from the protonosphere (H^+) component. It must be noticed that the negligible influence of the STEC from altitudes above the LEO satellite in the determination of the TI electron density has an important consequence for the estimated total electron content after integrating an RO-retrieved profile, since such an estimate will significantly deviate from the actual value of the total electron content.

[51] For the sample of electron density profiles analyzed in this study, the STIP model performs significantly better than the other classical functions considered, reducing the average differences between the fits and the observations to less than 4% in most cases. Generally, the STIP model achieves more than a factor of 2 improvement relative to the single component model functions represented by equations (8) to (10), as shown by the results of the comparisons reported in section 4.

[52] The results obtained in this work strongly support the assertion that the TI can be described using two essentially isothermal components which are modeled by the two terms of the STIP model function. Namely, an exponential term with a constant scale height describing the O^+ density, plus a constant term corresponding to the contribution of the H^+ density. In particular, the H^+ ion is generally an important component of the TI, reaching the largest densities for low geomagnetic latitudes and during sunlight local times. This has relevant implications for models of the ionosphere that rely on ionosonde measurements to compute the total electron content, that is, such models would be substantially biased if they do not take into account the contribution of the H^+ density.

[53] The altitude variation of the VSH inferred from the STIP model fits is also consistent with the empirical derivation of the VSH from the observed $N_e(h)$ profiles, implying that the model is also sensitive to the plasma temperature variations traced by the variations of the VSH. Therefore, the temperature variation in the TI will be essentially driven by the changes in the ratio between abundances of the two main ion constituents of that region. This last claim is strengthened by findings from the study of the correlation between H_s and H_u, which, for our sample of profiles, have been shown to be fully consistent with the results achieved by a previous study that used a completely different data set, methodology, and that covered a different epoch range. We have also shown that, without filtering the data by geomagnetic latitude, local time or season, the correlation between H_s and H_u is still significant and that, in fact, it arises from the correlation between the density parameters A and B that measure, in a global way, the contribution of each TI component to the electron density profile in the altitude range considered by the STIP-model fits.

[54] To sum up, despite its simplicity, the STIP model has been demonstrated to be a useful and accurate tool to explore and characterize the ionosphere/protonosphere interplay and, in particular, the distributions of the O^+ scale height and the UTH that can be easily calculated using the accurate fits to the observed $N_e(h)$ profiles. Subsequently, the parameters of the STIP model could be used to perform an analysis of the contribution made to the ionosphere composition by other ion species not considered by the model, particularly at altitudes below the TI. An interesting topic for future research will be to analyze whether the STIP model can be applied in other regions of the TI not covered by the present study, and even to consider the possibility of including the altitudes around the F2 peak, for example, replacing the exponential term in equation (1) by a Chapman function.

[55] **Acknowledgments.** The authors would like to express their gratitude to the University Corporation for Atmospheric Research and the National Space Organization in Taiwan for making available the FORMOSAT-3/COSMIC constellation data. This work has been supported by the Spanish Ministry of Science and Innovation under project CTM2010-21312-C03-02.

[56] Robert Lysak thanks the reviewers for their assistance in evaluating this paper.

References

Bilitza, D., and B. W. Reinisch (2007), International reference ionosphere 2007: Improvements and new parameters, *Adv. Space Res.*, *42*, 599–609.

Bishop, G. J., J. A. Secan, and S. H. Delay (2009), GPS TEC and the plasmasphere: Some observations and uncertainties, *Radio Sci.*, *44*, RS0A26, doi:10.1029/2008RS004037.

Cueto, M., P. Coïsson, S. M. Radicella, M. Herraiz, L. Ciraolo, and C. Brunini (2007), Topside ionosphere and plasmasphere: Use of NeQuick in connection with Gallagher plasmasphere model, *Adv. Space Res.*, *39*, 739–743.

Hernández-Pajares, M., J. M. Juan, and J. Sanz (2000), Improving the Abel inversion by adding ground GPS data to LEO radio occultation in ionospheric sounding, *Geophys. Res. Lett.*, *27*(16), 2473–2476.

Hysell, D. L., J. L. Chau, and J. D. Huba (2009), Topside measurements at Jicamarca during solar minimum, *Ann. Geophys.*, *27*, 427–439.

Kutiev, I. S., P. G. Marinov, and S. Watanabe (2006), Model of topside ionosphere scale height based on topside sounder data, *Adv. Space Res.*, *37*, 943–950.

Kutiev, I. S., and P. G. Marinov (2007), Topside sounder model of scale height and transition height characteristics of the ionosphere, *Adv. Space Res.*, *39*, 759–766.

Lee, H.-B., G. Jee, Y. H. Kim, and J. S. Shim (2013), Characteristics of global plasmaspheric TEC in comparison with the ionosphere simultaneously observed by Jason-1 satellite, *J. Geophys. Res. Space Physics*, *118*, 935–946, doi:10.1002/jgra.50130.

Lei, J., L. Liu, and W. Wan (2005), Variations of electron density based on long-term incoherent scatter radar and ionosonde measurements over Millstone Hill, *Radio Sci.*, *40*, RS2008, doi:10.1029/2004RS003106.

Liu, L., W. Wan, M. P. Sulzer, J. Lei, and M.-L. Zhang (2007a), An analysis of the scale heights in the lower topside ionosphere based on the Arecibo incoherent scatter radar measurements, *J. Geophys. Res.*, *112*, A06307, doi:10.1029/2007JA012250.

Liu, L., W. Wan, M.-L. Zhang, B. Ning, S.-R. Zhang, and J. M. Holt (2007b), Variations of topside ionospheric scale heights over Millstone Hill during the 30-day incoherent scatter radar experiment, *Ann. Geophys.*, *25*, 2019–2027.

Liu, L., M. He, W. Wan, and M.-L. Zhang (2008), Topside ionospheric scale heights retrieved from Constellation Observing System for Meteorology, Ionosphere and Climate radio occultation measurements, *J. Geophys. Res.*, *113*, A10304, doi:10.1029/2008JA013490.

Marinov, P., I. S. Kutiev, and S. Watanabe (2004), Empirical model of O^+/H^+ transition height based on topside sounder data, *Adv. Space Res.*, *34*, 2015–2022.

Mazzella Jr., A. J. (2009), Plasmasphere effects for GPS TEC measurements in North America, *Radio Sci.*, *44*, RS5014, doi:10.1029/2009RS004186.

Reinisch, B. W., P. Nsumei, X. Huang, and D. K. Bilitza (2007), Modeling the F2 topside and plasmasphere for IRI using IMAGE/RPI and ISIS data, *Adv. Space Res.*, *39*, 731–738.

Sibanda, P., and L. A. McKinnell (2011), Topside ionospheric vertical electron density profile reconstruction using GPS and ionosonde data: Possibilities for South Africa, *Ann. Geophys.*, *29*, 229–236, doi:10.5194/angeo-29-229-2011.

Stankov, S. M., and N. Jakowski (2006), Topside ionospheric scale height analysis and modelling based on radio occultation measurements, *J. Atmos. Solar-Terr. Phys.*, *68*, 134–162.

Stankov, S. M., P. G. Marinov, and I. S. Kutiev (2007), Comparison of NeQuick, PIM, and TSM model results for the topside ionospheric plasma scale and transition height, *Adv. Space Res.*, *39*, 767–773.

Stankov, S. M., K. Stegen, P. Muhtarov, and R. Warnant (2011), Local ionospheric electron density profile reconstruction in real time from simultaneous ground-based GNSS and ionosonde measurements, *Adv. Space Res.*, *47*, 1172–1180.

Webb, P. A., R. F. Benson, and J. M. Grebowsky (2006), Technique for determining midlatitude O^+/H^+ transition heights from topside ionograms, *Radio Sci.*, *41*, RS6S34, doi:10.1029/2005RS003391.

Yizengaw, E., M. B. Moldwin, D. Galvan, B. A. Iijima, A. Komjathy, and A. J. Mannucci (2008), Global plasmaspheric TEC and its relative contribution to GPS TEC, *J. Atmos. Solar-Terr. Phys.*, *70*, 1541–1548, doi:10.1016/j.jastp.2008.04.022.

Yue, X., W. S. Schreiner, J. Lei, C. Rocken, Y.-H. Kuo, and W. Wan (2010), Climatology of ionospheric upper transition height derived from COSMIC satellites during the solar minimum of 2008, *J. Atmos. Solar-Terr. Phys.*, *72*, 1270–1274, doi:10.1016/j.jastp.2010.08.018.